Inorganic Chemistry
Article

Inorg. Chem. **2011**, *50*, 545–558 **545**
DOI: 10.1021/ic101534n

Synthesis, Electronic Structure, DNA and Protein Binding, DNA Cleavage, and Anticancer Activity of Fluorophore-Labeled Copper(II) Complexes

Satish S. Bhat,[†] Anupa A. Kumbhar,*[,†] Hussain Heptullah,[‡] Ayesha A. Khan,[‡] Vivekanand V. Gobre,[†] Shridhar P. Gejji,[†] and Vedavati G. Puranik[§]

[†]*Department of Chemistry, University of Pune, Pune 411007, India,* [‡]*Institute of Bioinformatics and Biotechnology, University of Pune, Pune 411007, India, and* [§]*Centre for Materials Characterization, National Chemical Laboratory, Pune 411 008, India*

Received July 30, 2010

Two mononuclear fluorophore-labeled copper(II) complexes $[Cu(nip)(acac)]^{+}$(**2**) and $[Cu(nip)_2]^{2+}$ (**3**), where fluorophore is 2-(naphthalen-1-yl)-*1*H-imidazo[4,5-*f*][1,10]phenanthroline (nip) (**1**) and acac is acetylacetone, have been synthesized and characterized by various techniques. The ligand **1** and complex **2** are structurally characterized by single-crystal X-ray diffraction. The coordination geometries around the copper are square planar in solid as well as solution state as evidenced by electron paramagnetic resonance (EPR) spectroscopy. The density functional calculations carried out on **1**−**3** have shown that electron-rich regions in the highest occupied orbital are localized on the naphthalene and partly on the phenanthroline moiety. Both complexes **2** and **3** in dimethyl sulfoxide (DMSO) exhibit near square planar structure around the metal ion in their ground state. Time-dependent density functional theory (TD-DFT) calculations reveal that Cu(II) ion in complex **2** shows tetrahedral coordination around the metal while **3** retains its square planar geometry in the lowest excited state. The interaction of complexes with calf-thymus DNA (CT DNA) has been explored by using absorption, emission, thermal denaturation, and viscosity studies, and the intercalating mode of DNA binding has been proposed. The complexes cleave DNA oxidatively without any exogenous additives. The protein binding ability has been monitored by quenching of tryptophan emission in the presence of complexes using bovine serum albumin (BSA) as model protein. The compounds showed dynamic quenching behavior. Further, the anticancer activity of the complexes on MCF-7 (human breast cancer), HeLa (human cervical cancer), HL-60 (human promyelocytic leukemia), and MCF-12A (normal epithelial) cell lines has been studied. It has been observed that **3** exhibits higher cytotoxicity than **2**, and the cells undergo apoptotic cell death.

Introduction

Transition metal complexes play an important role in nucleic acids chemistry for their diverse applications such as footprinting agents, sequence specific binding, structural probes, and therapeutic agents.[1−5] Cisplatin [*cis*-diammino dichloroplatinum(II)][6−8] is one of the foremost and widely used metal-based anticancer drugs for cancer therapy, but it possesses inherent limitations such as serious side effects, general toxicity, and acquired drug resistance. Therefore, considerable attempts are being made to replace this drug with suitable alternatives, and numerous transition metal complexes have been synthesized and tested for their anticancer activities. Copper(II) complexes are regarded as the most promising alternatives to cisplatin as anticancer drugs.

Copper being a bioessential transition metal ion, its complexes with tunable coordination geometries in a redox active environment could find better applications at the cellular level. Sigman and co-workers[9] have developed the first chemical nuclease, bis-(1,10-phenanthroline) copper(I) complex, that effectively cleaves DNA in the minor groove in the presence of hydrogen peroxide. Recently there has been a substantial increase in the design and study of DNA binding and cleavage properties of mixed ligand copper(II) complexes[10−17] and development of new copper-based metallodrugs. Sadler and

*To whom correspondence should be addressed. E-mail: aak@chem.unipune.ac.in. Fax: (+91)-020 - 25691728.

(1) Metcalfe, C.; Thomas, J. A. *Chem. Soc. Rev.* **2003**, *32*, 215–224.
(2) Erkkila, K. E.; Odom, D. T.; Barton, J. K. *Chem. Rev.* **1999**, *99*, 2777–2795.
(3) Barton, J. K. *Science* **1986**, *233*, 727–734.
(4) Armitage, B. *Chem. Rev.* **1998**, *98*, 1171–1200.
(5) David, R.; McMillin, D. R.; McNett, K. M. *Chem. Rev.* **1998**, *98*, 1201–1220.
(6) Boulikas, T.; Vougiouka, M. *Oncol. Rep.* **2003**, *10*, 1663–1682.
(7) Wong, E.; Giandomenico, C. M. *Chem. Rev.* **1999**, *99*, 2451–2466.
(8) Jamieson, E. R.; Lippard, S. J. *Chem. Rev.* **1999**, *99*, 2467–2498.
(9) Sigman, D. S.; Mazumder, A.; Perrin, M. D. *Chem. Rev.* **1993**, *93*, 2295–2316.
(10) Barve, A.; Kumbhar, A.; Bhat, M.; Joshi, B.; Butcher, R.; Sonawane, U.; Joshi, R. *Inorg. Chem.* **2009**, *48*, 9120–9132.
(11) Chikira, M.; Tomizava, Y.; Fukita, D.; Sugizaki, T.; Sugawara, N.; Yamazaki, T.; Sasano, A.; Shindo, S.; Palaniandavar, M.; Anthroline, W. E. *J. Inorg. Biochem.* **2002**, *89*, 163–173.

Published on Web 12/14/2010

co-workers[18] have prepared mixed ligand bis(salicylato)-copper(II) complexes with diimine as coligands, which exhibit cytotoxic and antiviral activities. Recently Ademir Neves and co-workers have synthesized *cis*-aqua/hydroxyl copper(II) complexes containing tridentate ligands that are capable of promoting phosphate diester hydrolysis and DNA damage.[19] Reedijk and co-workers[20] have reported a [Cu^{II}(pyrimol)Cl] complex that catalytically cleaves target DNA in the absence of reductant at multiple positions of the nucleotide. Very recently, Palaniandavar et al.[21,22] reported mixed ligand copper(II) complexes of diimines containing phenolates and amino acids as coligands, which bind and cleave DNA and also exhibit anticancer activity. A substantial work on Co(III) and Ru(II) complexes of substituted-imidazo[4,5-*f*][1,10]phenanthroline has been reported by L.N. Ji et al.,[23−30] but to our knowledge, to date, there are no reports on Cu(II) complexes of these series of ligands.

Most of the reported copper-based complexes are not intrinsically fluorescent, so they need to be modified with a fluorescent tag in order to be visualized within the cells. This approach has been found to be useful in studying the cellular responses of several fluorescent platinum(II) and platinum(IV) complexes.[31−38] These compounds provided good resolution and clear identification of location of these compounds in subcellular organelles.

Here, we report the complexes of a fluorescent ligand (nip, **1**) that on complexation with Cu(II) makes the complexes fluorescent, so that we can monitor the cell penetration and distribution of these compounds in cancer cells using fluorescence microscopy. Because DNA and protein are the main cellular targets for the anticancer activity, DNA cleavage, and DNA and protein binding studies of these complexes by UV−visible and fluorescence spectroscopy have been carried out. The compounds have also been tested for their anticancer activity on a panel of cell lines. The mode of cell death was studied using DNA ladder and mitochondrial membrane permeability studies.

Experimental Section

Reagents and Materials. All reagents and solvents were purchased commercially and were used as received. Copper(II) nitrate trihydrate, 1,10-phenanthroline monohydrate, and ammonium acetate were purchased from S.D. Fine chemicals (India); calf thymus DNA and bovine serum albumin (BSA, fraction V) were purchased from SRL (India); supercoiled plasmid pBR322 DNA was obtained from Bangalore Genei (Bangalore, India).

Synthesis. 1,10-Phenanthroline-5,6-dione was synthesized according to a literature procedure.[39]

Synthesis of 2-(Naphthalen-1-yl)-1*H*-imidazo[4,5-*f*][1,10]phenanthroline (nip) (1). This compound was synthesized according to a literature procedure with minor modifications.[40] A mixture of 1-naphthaldehyde (0.372 g, 2.38 mM), 1,10-phenanthroline-5,6-dione (0.500 g, 2.38 mM), and ammonium acetate (0.367 g, 4.76 mM) in glacial acetic acid (10 mL) was refluxed for about 2 h, then cooled to room temperature and diluted with water (40 mL). Dropwise addition of diluted aqueous ammonia gave a yellow precipitate, which was collected and washed with water. The crude product was purified by column chromatography (SiO_2, $CHCl_3$/MeOH). Yield: 0.717 g (87%). ^{1}H NMR (DMSO-d_6, 300 MHz, 25 °C): δ = 13.96 (br, 1H), 9.125 (1H, d), 9.062 (2H, d), 8.97 (2H, d), 8.126(3H, m), 7.85 (2H, m), 7.701 (3H, m). IR (KBr pellet, cm^{-1}): ν = 3140 (NH), 3051, 2956 (CH), 1612 (C=N), 1579, 1564, 1462, 1410 (C=C). Anal. Calcd for (%) for $C_{23}H_{14}N_4 \cdot 0.25CHCl_3$: C, 74.22; H, 3.82; N, 14.80. Found: C, 74.53, H, 3.97, N, 14.71.

Synthesis of [Cu(acac)(nip)](NO_3) (2). This complex was prepared by addition of a methanolic solution of nip (0.200 g, 0.577 mM) and acetylacetone (0.0578 g, 0.577 mM) to a solution of copper(II) nitrate trihydrate (0.139 g, 0.577 mM) in methanol and then refluxed for 5−6 h. The solution was cooled to room temperature, filtered, and allowed to stand for evaporation at room temperature. After several days, brownish green crystals suitable for X-ray crystallography were obtained. Yield: 0.272 g (83%). IR (KBr pellet, cm^{-1}) ν = 3412 (H_2O), 3052, 3020 (ArH), 2949, 2862 (CH_2), 1579, 1566, 1458, 1425 (C=C, C=N). ESI-MS (m/z, positive mode): ($[M - NO_3]^+$) 509., Anal. Calcd for (%) for

(12) Selvakumar, B.; Rajendiran, V.; Maheswari, P. U.; Evans, H. S.; Palaniandavar, M. *J. Inorg. Biochem.* **2006**, *100*, 316–330.
(13) Reddy, P. A. N.; Nethaji, M.; Chakravarty, A. R. *Eur. J. Inorg. Chem.* **2004**, 1440–1446.
(14) Rossi, M. L.; Neves, A.; Bortoluzzi, A. J.; Horner, R.; Szpoganicz, B.; Terenzi, H.; Mangrich, A. S.; Pereira-Maia, E.; Castellano, E. E.; Haase, W. *Inorg. Chim. Acta* **2005**, *358*, 1807–1822.
(15) Bof Oliveira, M. C.; Mazera, D.; Scarpellini, M.; Severino, P. C.; Neves, A.; Terenzi, H. *Inorg. Chem.* **2009**, *48*, 2711–2713.
(16) Barcelo-Oliver, M.; Garcıa-Raso, A. Ä .; Terron, A Ä.; Molins, E.; Prieto, M. J.; Moreno, V.; Martınez, J.; Llado, V.; Lopez, I.; Gutierrez, A.; Escriba, P. V. *J. Inorg. Biochem.* **2007**, *101*, 649–659.
(17) Garcıa- Raso, A. Ä .; Fiol, J. J.; Adrover, B.; Moreno, V.; Mata, I.; Espinso, E.; Molins, E. *J. Inorg. Biochem.* **2003**, *95*, 77–86.
(18) Ranford, J. D.; Sadler, P. J.; Tocher, D. A. *Dalton Trans.* **1993**, 3393–3399.
(19) Scarpellini, M.; Neves, A.; Horner, R.; Bortoluzzi, A. J.; Szpoganicz, B.; Zucco, C.; Silva, R. A. N.; Drago, V.; Mangrich, A. S.; Ortiz, W. A.; Passos, A. C. W.; Oliveira, M. C. B.; Terenzi, H. *Inorg. Chem.* **2003**, *42*, 8353–8365.
(20) Maheswari, P. U.; Roy, S.; den Dulk, H.; Barends, S.; van Wezel, G.; Kozlevcar, B.; Gamez, P.; Reedijk, J. *J. Am. Chem. Soc.* **2006**, *128*, 710–711.
(21) Ramakrishnan, S.; Rajendiran, V.; Palaniandavar, M.; Periasamy, V. S.; Srinag, B. S.; Krishnamurthy, H.; Akbarsha, M. A. *Inorg. Chem.* **2009**, *48*, 1309–1322.
(22) Rajendiran, V.; Karthik, R.; Palaniandavar, M.; Evans, H. S.; Periasamay, V. S.; Akbarsha, M. A.; Srinag, B. S.; Krishnamurthy, H. *Inorg. Chem.* **2007**, *46*, 8208–8221.
(23) Liu, Y.-J.; Chao, H.; Yuan, Y.-X.; Yu, H.-J.; Ji, L.-N. *Inorg. Chem. Acta* **2006**, *359*, 3807–3814.
(24) Tan, Li-F.; Liu, Xiao-Hua.; Chao, H.; Ji, L.-N. *J. Inorg. Biochem.* **2007**, *101*, 56–63.
(25) Sun, B.; Wang, Y.-C.; Qian, C.; Chu, J.; Liang, Si-M.; Chao, H.; Ji, L.-N. *J. Mol. Struct.* **2010**, *963*, 153–159.
(26) Tan, L.-F.; Chao, H.; Zhou, Y.-F.; Ji, L.-N. *Polyhedron* **2007**, *26*, 3029–3036.
(27) Tan, L.-F.; Chao, H.; Li, H.; Liu, Y.-J.; Sun, B.; Wei, W.; Ji, L.-N. *J. Inorg. Biochem.* **2005**, *99*, 513–520.
(28) Zhang, Q. L.; Liu, J.-G.; Liu, J.-Z.; Li, H.; Yang, Y.; Xu, H.; Chao, H.; Ji, L.-N. *Inorg. Chem. Acta* **2002**, *339*, 34–40.
(29) Zhanga, Q.-L.; Liua, J.-H.; Rena, X.-Z.; Xua, H.; Huanga, Y.; Liub, J.-Z.; Ji, L.-N. J. *Inorg. Biochem.* **2003**, *95*, 194–198.
(30) Tan, L.-F.; Chao, H.; Liu, Y.-J.; Hong, L.; Sun, B.; Ji, L.-N. *Inorg. Chem. Acta* **2005**, *358*, 2191–2198.
(31) Teicher, B. A.; Holden, S. A.; Jacobs, J. L.; Abrams, M. J.; Jones, A. G. *Biochem. Pharmacol.* **1986**, *35*, 3365–3369.
(32) Sandman, K. E.; Marla, S. S.; Zlokarnik, G.; Lippard, S. J. *Chem. Biol.* **1999**, *6*, 541–551.
(33) Molenaar, C.; Teuben, J.-M; Heetebrij, R. J.; Tanke, H. J.; Reedijk, J. *J. Biol. Inorg. Chem.* **2000**, *5*, 655–665.
(34) Safaei, R.; Katano, K.; Larson, B. J.; Samimi, G.; Holzer, A. K.; Naerdemann, W.; Tomioka, M.; Goodman, M.; Howell, S. B. *Clin. Cancer Res.* **2005**, *11*, 756–767.
(35) Liang, X.-J.; Shen, D.-W.; Chen, K. G.; Wincovitch, S. M.; Garfield, S. H.; Gottesman, M. M. *J. Cell. Physiol.* **2005**, *202*, 635–641.
(36) Kalayda, G. V.; Jansen, B. A. J.; Molenaar, C.; Wielaard, P.; Tanke, H. J.; Reedijk, J. *J. Biol. Inorg. Chem.* **2004**, *9*, 414–422.
(37) Jansen, B. A. J.; Wielaard, P.; Kalayda, G. V.; Ferrari, M.; Molenaar, C.; Tanke, H. J.; Brouwer, J.; Reedijk, J. *J. Biol. Inorg. Chem.* **2004**, *9*, 403–413.
(38) Kalayda, G. V.; Jansen, B. A. J.; Wielaard, P.; Tanke, H. J.; Reedijk, J. *J. Biol. Inorg. Chem.* **2005**, *10*, 305–315.
(39) Yamada, M.; Tanaka, Y.; Yoshimoto, Y.; Kuroda, S.; Shimao, I. *Bull. Chem. Soc. Jpn.* **1992**, *65*, 1006–1011.
(40) Shi, L.; Li, B. *Eur. J. Inorg. Chem.* **2009**, *15*, 2294–2302.

Table 1. Selected Crystallographic Data for **1** and **2**

empirical formula	$C_{23}H_{14}N_4$ (**1**)	$C_{28}H_{21}CuN_4O_2.NO_3$ (**2**)
formula weight	346.38	571.04
temp, K	296(2)	296(2)
wavelength, Å	0.71073	0.71073
cryst. syst., space group	monoclinic, $P2_1/c$	monoclinic, $P2_1/c$
unit cell dimensions	a = 16.236(2) Å, α = 90°	a = 7.1127(5) Å, α = 90°
	b = 7.4541(9) Å, β = 93.989(3)°	b = 14.5569(1) Å, β = 90.302(2)°
	c = 13.6519(17) Å, γ = 90°	c = 23.6079(18) Å, γ = 90°
vol, Å^3	1648.2(4)	2444.3(3)
Z, calcd density (g/cm^3)	4, 1.396	4, 1.554
abs. coeff., mm^{-1}	0.085	0.945
F(000)	720	1176
cryst. size, mm^3	0.23 × 0.09 × 0.02	0.25 × 0.16 × 0.14
θ range for data collection	2.52−23.74°	1.73−23.49°
reflns collected/unique	7167/2516 [R(int) = 0.0483]	20524/3601 [R(int) = 0.0875]
data/restraints/params	2516/0/244	3601/0/354
GOF on F^2	1.242	1.221
final R indices [$I > 2\sigma(I)$]	R1 = 0.0741, wR2 = 0.1510	R1 = 0.0846, wR2 = 0.1534
R indices (all data)	R1 = 0.1080, wR2 = 0.1632	R1 = 0.1125, wR2 = 0.1648

$C_{28}H_{21}N_5O_5Cu$: C, 58.91; H, 3.72; N, 12.26. Found: C, 58.88; H, 3.69; N, 12.01.

Synthesis of $[Cu(nip)_2](NO_3)_2$ (3). This complex was prepared by addition of a methanolic solution of nip (0.358 g, 1.03 mM) to a solution of copper(II) nitrate trihydrate (0.125 g, 0.51 mM) in methanol and then refluxed for 5−6 h. The solution was cooled to room temperature. The precipitate formed was collected by filtration and washed with small amounts of methanol/chloroform followed by diethyl ether. Yield: 320 mg (70.0%). IR (KBr pellet, cm^{-1}): ν = 3412 (H_2O), 3052, 3020 (ArH), 2949, 2862 (CH_2), 1579, 1566, 1458, 1425 (C═C, C═N). ESI-MS (m/z, positive mode): ($[M - NO_3]^+$), 818; ($[M - 2NO_3]^{2+}$), 378. Anal. Calcd for (%) for $C_{46}H_{28}N_{10}O_6Cu \cdot 0.5CHCl_3$: C, 59.41; H, 3.06; N, 14.90. Found: C, 59.25; H, 2.95; N, 14.75.

Methods and Instrumentation. Spectroscopy and Electrochemistry. ^{1}H NMR spectrum was recorded on a Varian-Mercury 300 MHz spectrometer with DMSO-d_6 as a solvent at room temperature, and all chemical shifts are given relative to TMS. The infrared spectra of solid samples dispersed in KBr were recorded on a Shimadzu FTIR-8400 spectrophotometer. The electrospray mass spectra were recorded on a MICROMASS QUATTRO II triple quadrupole mass spectrometer using methanol as solvent. The ESI capillary voltage was set at 3.5 kV, and the cone voltage was 40 V. UV−vis spectra were recorded on a Jasco UV−vis spectrophotometer in DMF. Steady-state emission experiments were carried out on a Shimadzu RF-5301 spectrofluorometer at room temperature in DMF. Microanalyses (C, H, and N) were carried out with a ThermoQuest microanalysis instrument capable of carrying out CHNS (carbon, hydrogen, nitrogen, and sulfur) analyses.

Electrochemistry of copper(II) complexes in dimethyl sulfoxide solution was performed under nitrogen atmosphere on a CH-electrochemical analyzer model 1100A with a conventional three-electrode cell assembly with a saturated Ag/AgCl reference electrode, glassy carbon electrode as working electrode and platinum wire as an auxiliary electrode for all measurements in the presence of tetraethyl ammonium perchlorate as supporting electrolyte.

Emission quantum yields (ϕ) were calculated by integrating the area under the fluorescence curves and by using eq 1.[41]

$$\phi_{sample} = \{OD_{standard}A_{sample}\}/\{OD_{sample}A_{standard}\}\phi_{standard} \quad (1)$$

where OD is optical density of the compound at the excitation wavelength and A is the area under the emission spectral curve. Anthracene was used as standard for the fluorescence quantum yield measurements. The quantum yields calculated were corrected for refractive index of solvent.

X-ray Crystallography. Data for both compounds were collected at T = 296 K, on SMART APEX CCD single-crystal X-ray diffractometer using Mo Kα radiation (λ = 0.7107 Å) to a maximum θ range of 25.00°. The structures were solved by direct methods using SHELXTL. All the data were corrected for Lorentzian, polarization and absorption effects. SHELX-97 (ShelxTL)[42] was used to solve the structure and full matrix least-squares refinement on F^2. Hydrogen atoms were included in the refinement as per the riding model. The refinements were carried out using SHELXL-97. Crystal parameters and details of the data collection and refinement are given in Table 1. Selected bond lengths and bond angles are given in Table S1 and S2, Supporting Information.

DNA Binding Studies. The concentration of CT-DNA was calculated from its known extinction coefficient at 260 nm (6600 M^{-1} cm^{-1}). Solutions of calf thymus DNA in phosphate buffer gave a ratio of UV absorbance at 260 and 280 nm (A_{260}/A_{280}) 1.8−1.9 indicating that the DNA was sufficiently free of protein.

Absorption titration experiments were performed by maintaining a constant metal complex concentration (20 μM) and varying nucleotide concentration (0−40 μM) in buffer. After addition of DNA to the metal complex, the resulting solution was allowed to equilibrate at 25 °C for 20 min, after which absorption readings were noted. The data were then fit to eq 2[43] to obtain intrinsic binding constant K_b.

$$[DNA]/[\varepsilon_a - \varepsilon_f] = [DNA]/[\varepsilon_b - \varepsilon_f] + 1/K_b[\varepsilon_b - \varepsilon_f] \quad (2)$$

where [DNA] is the concentration of DNA in base pairs, ε_a is the extinction coefficient observed for the MLCT absorption band at the given DNA concentration, ε_f is the extinction coefficient of the complex free in solution, and ε_b is the extinction coefficient of the complex when fully bound to DNA. A plot of $[DNA]/[\varepsilon_a - \varepsilon_f]$ versus [DNA] gave a slope $1/[\varepsilon_a - \varepsilon_f]$ and Y intercept equal to $(1/K_b)[\varepsilon_b - \varepsilon_f]$, respectively. The intrinsic binding constant K_b is the ratio of the slope to the intercept.[43]

Viscosity experiments were carried out using a semimicro-viscometer maintained at 28 °C in a thermostatic water bath. Flow time of solutions in phosphate buffer (pH 7.2) was recorded in triplicate for each sample and an average flow time was calculated. Data were presented as $(\eta/\eta^0)^{1/3}$ versus binding ratio, where η is the viscosity of DNA in the presence of complex and η^0 is the viscosity of DNA alone.

DNA melting experiments were carried out in phosphate buffer (pH 7.2) on a JASCO V-630 spectrophotometer equipped with a Peltier temperature-controlling programmer ETC-717 (±0.1 °C).

(41) Lakowicz, J. R. *Principles of Luminescence Spectroscopy*, 3rd ed.; New York, 2006.

(42) Sheldrick, G. M. *SHELX-97 program for crystal structure solution and refinement*, University of Gottingen, Germany, 1997.

(43) Wolfe, A.; Shimer, G. H.; Meehan, T. *Biochemistry* **1987**, *26*, 6392–6396.

UV melting profiles were obtained by scanning A_{260} absorbance monitored at a heating rate of 1 °C/min for solutions of CT DNA (100 μM) in the absence and presence of copper(II) complexes (20 μM) from 30 to 90 °C with the use of the thermal melting program. The melting temperature, T_m, which is defined as the temperature where half of the total base pairs are unbound, was determined from the midpoint of the melting curves.

Competitive Binding Fluorescence Measurements. The apparent binding constants (K_{app}) of the complexes were determined by a fluorescence spectral technique using ethidium bromide (EtBr)-bound CT DNA solution in phosphate buffer (pH, 7.2). The changes in fluorescence intensities at 600 nm (546 nm excitation) of EtBr bound to DNA were recorded with an increasing amount of the copper(II) complex concentration. EtBr was non-emissive in phosphate buffer (pH 7.2) due to fluorescence quenching of the free EtBr by the solvent molecules. In the presence of DNA, EtBr showed enhanced emission intensity due to its intercalative binding to DNA. A competitive binding of the copper complexes to CT DNA resulted in the displacement of the bound EtBr decreasing its emission intensity.

DNA Cleavage Studies. The DNA cleavage was carried out by agarose gel electrophoresis on a 10 μL total sample volume in 0.5 mL transparent Eppendorf microcentrifuge tubes containing pBR322 DNA (200 ng). For the gel-electrophoresis experiments, supercoiled pBR322 DNA was treated with the metal complexes (10−100 μM), and the mixtures were incubated in the dark for 30 min at 37 °C. The samples were analyzed by 1% agarose gel electrophoresis (Tris−boric acid−EDTA (TBE) buffer, pH = 8.2) for 3 h at 60 V. The gel was stained with 0.5 μg/mL ethidium bromide and visualized by UV light and photographed for analysis. The extent of cleavage of the SC DNA was determined by measuring the intensities of the bands using the Alpha Innotech gel documentation system (AlphaImager 2200). For mechanistic investigations, experiments were carried out in the presence of different radical scavenging agents. These reactions were carried out by adding scavenging agents such as DMSO, mannitol, DABCO, L-histidine, and SOD to SC DNA prior to the addition of the complexes. Samples were incubated for 30 min at 37 °C. The concentrations of scavenging agents given in parentheses (figure caption of Figure 10) correspond to stock concentration. One microliter of stock solution was added to make the total reaction volume 10 μL.

BSA Interaction Studies. Quenching of the tryptophan residues of BSA was performed using complexes **2** and **3** as quenchers. To solutions of BSA in phosphate buffer at pH 7.2, increments of the quenchers were added, and the emission signals at 344 nm (excitation wavelength at 295 nm) were recorded after each addition of the quencher.[22,44]

Anticancer Activity. Maintenance of Cancer Cell Lines. The cell lines MCF-7 (human breast cancer), HeLa (human cervical cancer), HL-60 (human promyelocytic leukemia), and MCF-12A (normal epithelial) were obtained from National Centre for Cell Sciences Repository, University of Pune, Pune, India. The cells were maintained in Dulbecco's minimum essential medium (DMEM) with 10% FBS and 0.1% antibiotic solution (complete medium-CM) at 37 °C at 5% CO_2 in the stericycle CO_2 incubator with HEPA class 100 filters, Thermo Electron Corporation.

Preparation of Samples for Cell Line Testing. The compounds **1**−**3** were dissolved in 20% DMSO to obtain a solution of 1 mM concentration each. These samples were then diluted to 100 μM in PBS solution and filter-sterilized using a 0.22 μm filter via syringe filter. This 100 μM solution in PBS was further used in cell cytotoxicity studies.

Testing of Compounds on Various Cell Lines. The cells, trypsinized using TPVG solution (1×10^5 cells/ml), were seeded in a 96-well plate. A range of concentrations of the compounds diluted in CM were added to the cells and incubated at 37 °C in a CO_2 incubator for 24, 48, 72, and 96 h. After the incubation, the cells were visualized using an inverted Olympus microscope. All experiments were carried out in laminar flow hoods, Laminar Flow Ultraclean Air Unit, Microfilt, India.

Protocol for MTT Assay. A solution of 5 mg/mL MTT was dissolved in PBS and filter-sterilized using a syringe filter. After incubation for the stipulated time, 20 μL of MTT solution was added to 200 μL of cell content solution. The plate was incubated for 2 h in the CO_2 incubator. After incubation, the media was removed, 200 μL of DMSO was added to each well to dissolve the crystals, and the plate was placed into the incubator at 37 °C for 5 min. A reading was taken on a plate reader, Thermo Electron Corporation, and absorbance was measured at 540 and 620 nm.

DNA Extraction Protocol. From cell lines preinoculated with compounds, a pellet of about 100 μL of cells was prepared, and supernatant was discarded. Cells were resuspended (on ice) in 20 μL of lysis buffer, and 5 μL of proteinase k solution was added. Cells were pipetted to ensure complete lysis and incubated at 55 °C for 1 h. A pellet of cell debris was made, and then 5 μL of RNase A was added to the supernatant. It was incubated for another hour at 55 °C. Samples were spun briefly to sediment any other cell debris, and the supernatant was collected. Samples were stored at −20 °C for further use.

Agarose gel (0.8%) was run at 40 V, and EtBr staining and de-staining was performed.

RNase Solution. RNase (1 mg/mL) in molecular grade water (DEPC water) was heated to 100 °C to ensure that all DNase activity was destroyed.

Proteinase k. Proteinase k powder (1 mg/mL) was added to 1 mL of molecular grade water (DEPC water).

Lysis Buffer. Lysis buffer consisted of 50 mM tris-HCl (pH 8.0), 10 mM EDTA, 0.5% SDS, and 0.5 mg/mL proteinase k added fresh.

For preparation for fluorescent images (from cell lines preinoculated with compounds, in 24 well plate), 100 μL of cell content was pipetted out and centrifuged at 5000 rpm for 10 min. Cells were briefly washed with PBS twice. The pellet was resuspended in 50 μL of PBS. Ten microliters of the suspended cells was placed on a clean glass slide, and a coverslip was imposed in such a way that no air bubbles were obtained. Images were taken in a Carl Zeiss Axio Scope A1 fluorescence microscope with filter set no. 9 and excitation at 450−490 nm.

Computational Method. Geometry optimizations of **1**−**3** have been carried out using the hybrid density functional theory incorporating the Becke's three parameter exchange (B3) with Lee, Yang, and Parr (LYP) correlation functional[45] employing the Gaussian 09 program.[46] The internally stored 6-31G(d, p) basis set was employed. Stationary point geometries thus obtained were characterized as local minima on the potential energy surface since all the frequencies of normal vibrations for these structures turn

(44) Quiming, N. S.; Vergel, R. B.; Nicolas, M. G.; Villanueva, J. A. *J. Health Sci.* **2005**, *51*, 8–15.

(45) Lee, C.; Yang, W.; Parr, R. G. *Phys. Rev. B* **1988**, *37*, 785–789.

(46) Frisch, M. J.; Trucks, G. W.; Schlegel, H. B.; Scuseria, G. E.; Robb, M. A.; Cheeseman, J. R.; Scalmani, G.; Barone, V.; Mennucci, B.; Petersson, G. A.; Nakatsuji, H.; Caricato, M.; Li, X.; Hratchian, H. P.; Izmaylov, A. F.; Bloino, J.; Zheng, G.; Sonnenberg, J. L.; Hada, M.; Ehara, M.; Toyota, K.; Fukuda, R.; Hasegawa, J.; Ishida, M.; Nakajima, T.; Honda, Y.; Kitao, O.; Nakai, H.; Vreven, T.; Montgomery, J. A., Jr.; Peralta, J. E.; Ogliaro, F.; Bearpark, M.; Heyd, J. J.; Brothers, E.; Kudin, K. N.; Staroverov, V. N.; Kobayashi, R.; Normand, J.; Raghavachari, K.; Rendell, A.; Burant, J. C.; Iyengar, S. S.; Tomasi, J.; Cossi, M.; Rega, N.; Millam, J. M.; Klene, M.; Knox, J. E.; Cross, J. B.; Bakken, V.; Adamo, C.; Jaramillo, J.; Gomperts, R.; Stratmann, R. E.; Yazyev, O.; Austin, A. J.; Cammi, R.; Pomelli, C.; Ochterski, J. W.; Martin, R. L.; Morokuma, K.; Zakrzewski, V. G.; Voth, G. A.; Salvador, P.; Dannenberg, J. J.; Dapprich, S.; Daniels, A. D.; Farkas, O.; Foresman, J. B.; Ortiz, J. V.; Cioslowski, J.; Fox, D. J. *Gaussian 09*, revision A.02; Gaussian, Inc.: Wallingford, CT, 2009.

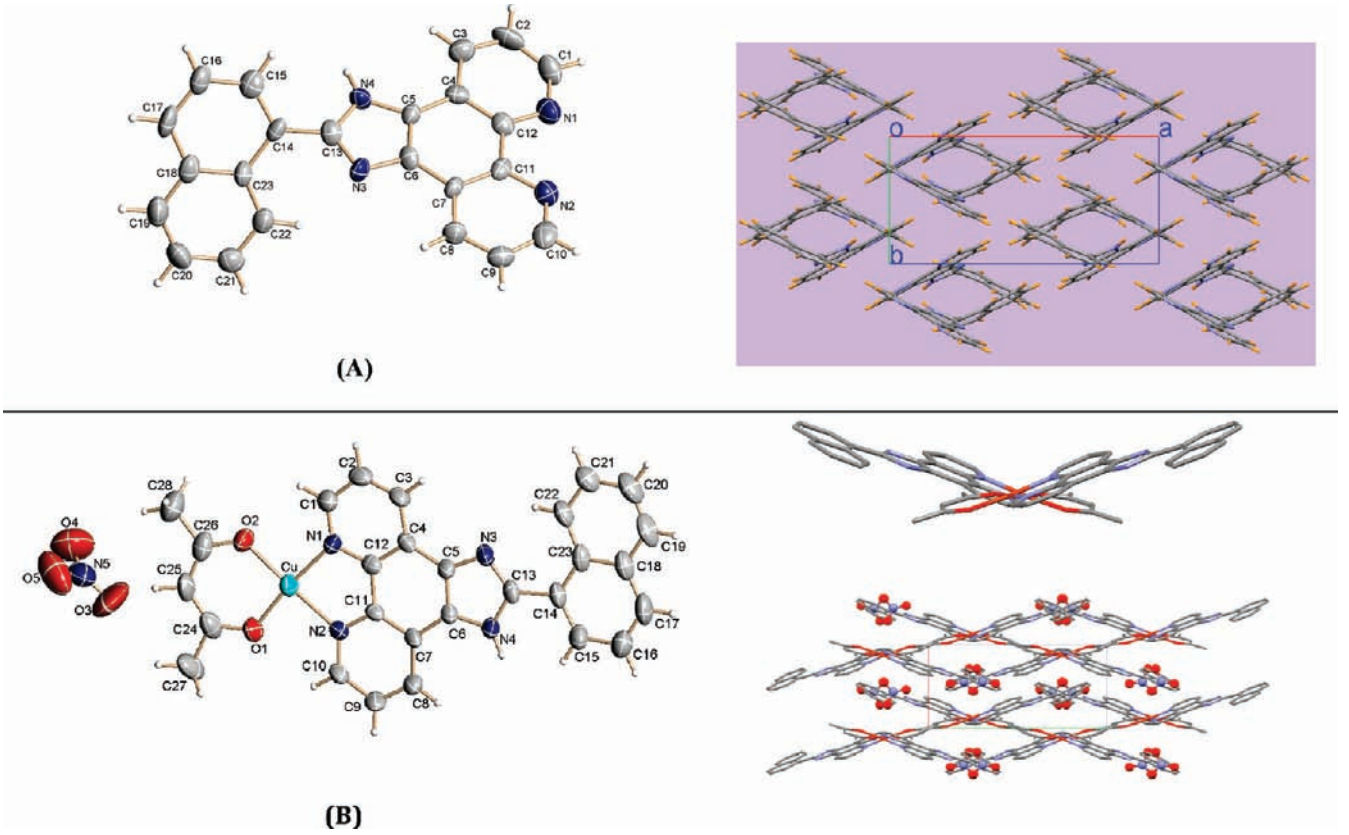

Figure 1. ORTEP and packing diagram of (**A**) **1** and (**B**) **2**. Ellipsoids are drawn at 50% probability.

Scheme 1. Synthetic Route for Complexes **2** and **3**

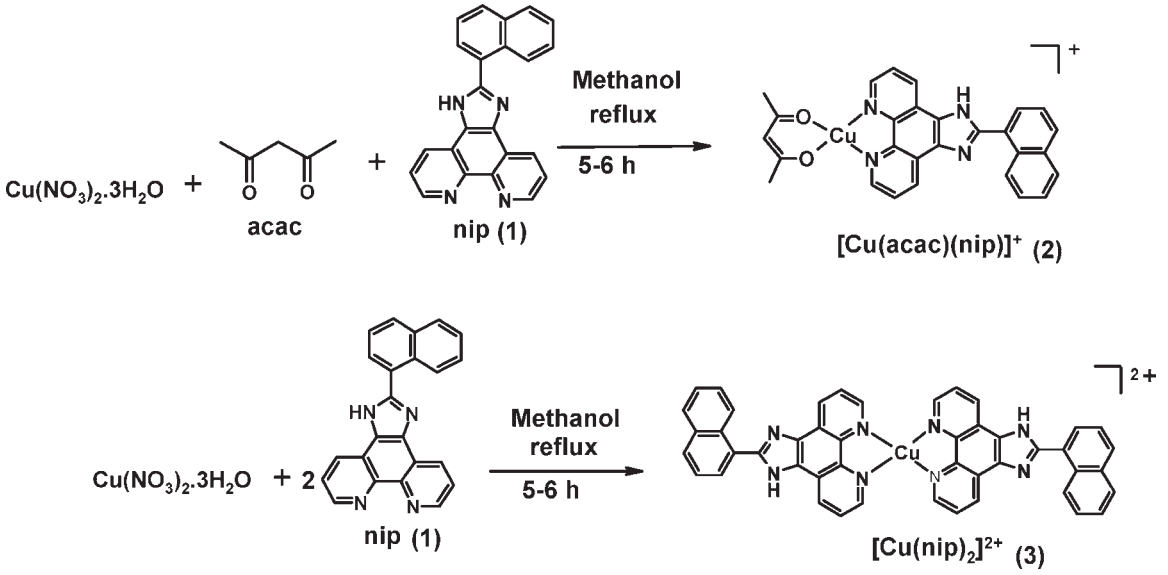

out to be real. The influence of dimethylsulfoxide (DMSO) solvent on the structure of the complex was modeled through the self-consistent reaction field theory incorporating the polarizable continuum model.[47]

Result and Discussions

Synthesis and Characterization. The phenanthroline-based ligand nip (**1**) was prepared by condensation of 1,10-phenanthroline-5,6-dione and 1-naphthaldehyde in the presence of ammonium acetate in glacial acetic acid. Its structure was confirmed by elemental analysis, ESI-MS, ^{1}H NMR, and single-crystal X-ray structure. The ^{1}H NMR spectrum of the nip ligand displays a broad peak at 13.96 ppm, which can be assigned to the N−H proton from the imidazole ring. The corresponding copper(II) complexes were synthesized as described in the Experimental Section (Scheme 1). The complexes were obtained in good yield and characterized by IR, Elemental analysis,

(47) Miiertus, S.; Scrocco, E.; Tomasi *J. Chem. Phys.* **1981**, *55*, 117–129.

Table 2. UV−Visible and Emission Data for **1**−**3**

compound[a]	absorbance[b], λ_{max} (nm) (ε (M^{-1} cm^{-1}))		emission[b]	
	ligand transitions	MLCT	λ_{em} (nm)	ϕ_{em}[c]
nip (**1**)	325 (24220), 287 (35220)		433	0.629
[Cu(acac)(nip)](NO_3) (**2**)	346 (27640), 284 (36600)	700(38.3)	429	0.147
[Cu(nip)$_2$](NO_3)$_2$ (**3**)	338(50040), 285 (65940), 266 (64860)	690(76.3)	432	0.29

[a] [**1**−**3**] = 10 μM. [b] Spectra were recorded in DMF at 298 K. [c] ϕ_{em} = emission quantum yield. Error limit: λ_{max} = ±2 nm, λ_{em} = ±2 nm, ϕ_{em} = ±5%

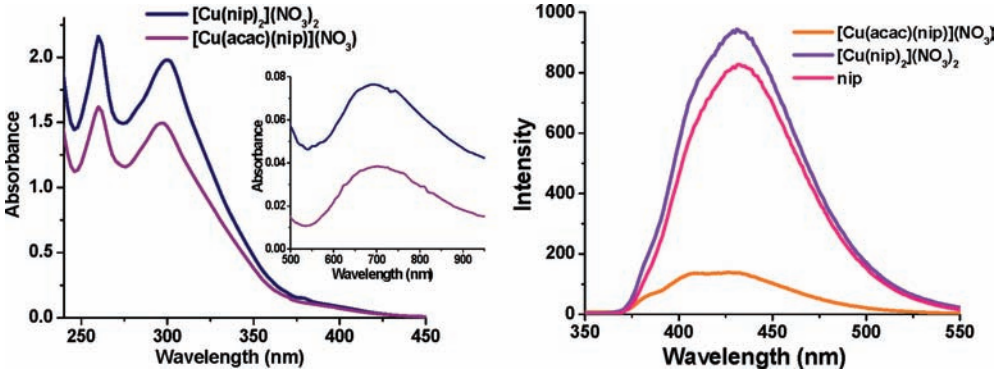

Figure 2. UV−visible and emission spectra of **1**−**3** (10 μM) in DMF.

electrochemistry, UV−visible, fluorescence spectroscopy, EPR, and electrospray ionization mass spectrometry (see Experimental Section). In ESI-MS, peaks due to $[M - (NO_3)]^+$ and $[M - 2(NO_3)]^{2+}$ were observed. The compounds **1** and **2** were also characterized by single-crystal X-ray structure.

Crystal Structure. Single crystals of **1** suitable for X-ray diffraction were grown by slow evaporation of the compound in dimethyl formamide at room temperature. The compound crystallizes in the monoclinic space group $P2_1/c$. An ORTEP representation of **1** is shown in Figure 1A. A summary of the crystallographic data is compiled in Table 1; bond lengths and bond angles for **1** are given in Table S1, Supporting Information. The naphthalene ring is at an angle to the phenanthroline ring. It shows a diamond-like packing arrangement when viewed down the *c* axis (Figure 1), and the two molecules are held by $\pi-\pi$ interactions (Supporting Information, Figure S1).

A single crystal of **2** suitable for X-ray diffraction was grown by slow evaporation of the compound in methanol at room temperature. The compound crystallized in monoclinic space group $P2_1/c$. The ORTEP representation of **2** with atom numbering scheme is shown in Figure 1B. Here the Cu(II) atom is coordinated to one acetylacetone through oxygen atoms and to one nip ligand through the nitrogen atoms. A summary of the crystallographic data is compiled in Table 1, and selected bond lengths and bond angles are given in Supporting Information (Table S2). When **1** forms a complex with copper(II), the naphthalene ring rotates through 49.43° to form hydrogen bonds with lattice nitrates (Overlap of the **1** and **2** is shown in Supporting Information, Figure S3). The X-ray analysis shows that the complex **2** crystallizes along with NO_3 anion and has a planar conformation.

The average Cu−N bond distance is 1.998(5) Å and Cu−O bond distance is 1.891(4) Å. These distances are found to be similar to that of CuN_2O_2-type of complexes reported in the literature.[10,48] Planar nip ligands of neighboring cations are held together by $\pi-\pi$ interactions, while the NO_3 anion connects the symmetry-related molecules via C−H···O and C−H···N interactions (Supporting Information, Figures S2 and S3). The cationic units in **2** are arranged in a zigzag manner (Figure 1B), in such a way that the phenanthroline moieties of the adjacent cationic units are exactly opposite and perpendicular to each other (Supporting Information, Figure S2) and the two ligands hydrogen bond with the ligands of the adjacent cationic molecules maximizing the number of hydrogen bonds with each other in order to stabilize the structure. The cations are surrounded by nitrate anions and show a network of H-bonding.

Photophysical Studies. The photophysical properties of complexes **2** and **3** are summarized in Table 2. The UV−visible spectra of ligand and complexes recorded in dimethylformamide (DMF) are dominated by high-energy bands between 240 to 400 nm corresponding to $\pi \rightarrow \pi^*$ transitions of the aromatic nitrogen donor ligands. The low-energy bands around 700 nm for **2** and **3** are assigned as the (dπ) → ligand (π^*) transitions typical of copper(II) complexes.[10,22]

The excitation of the band at 330 nm of **1**−**3** in DMF at room temperature results in an intense emission peak centered between 380 and 550 nm (Figure 2). The emission maxima, relative quantum yields, and lifetimes are compiled in Table 2. Interestingly, it has been observed that there is drastic quenching of fluorescence intensity in **2** as compared with **1** (6-fold) and **3** (7-fold). The only difference between **2** and **3** is that **2** contains an acetylacetone moiety as an ancillary ligand (N_2O_2 coordination), while **3** has two nip ligands (N_4 coordination). This suggests that quenching is a coordination-mediated event. As per earlier literature by Shi and Li,[40] planarity between the imidazo[4,5-*f*]-[1,10]phenanthroline and naphthalene moiety should enhance the fluorescence. However, our observation

(48) Onawumi, E. O.O.; Faboya, O. O. P.; Odunola, A. O.; Prasad, T. K.; Rajasekharan, M. V. *Polyhedron* **2008**, *27*, 113–117.

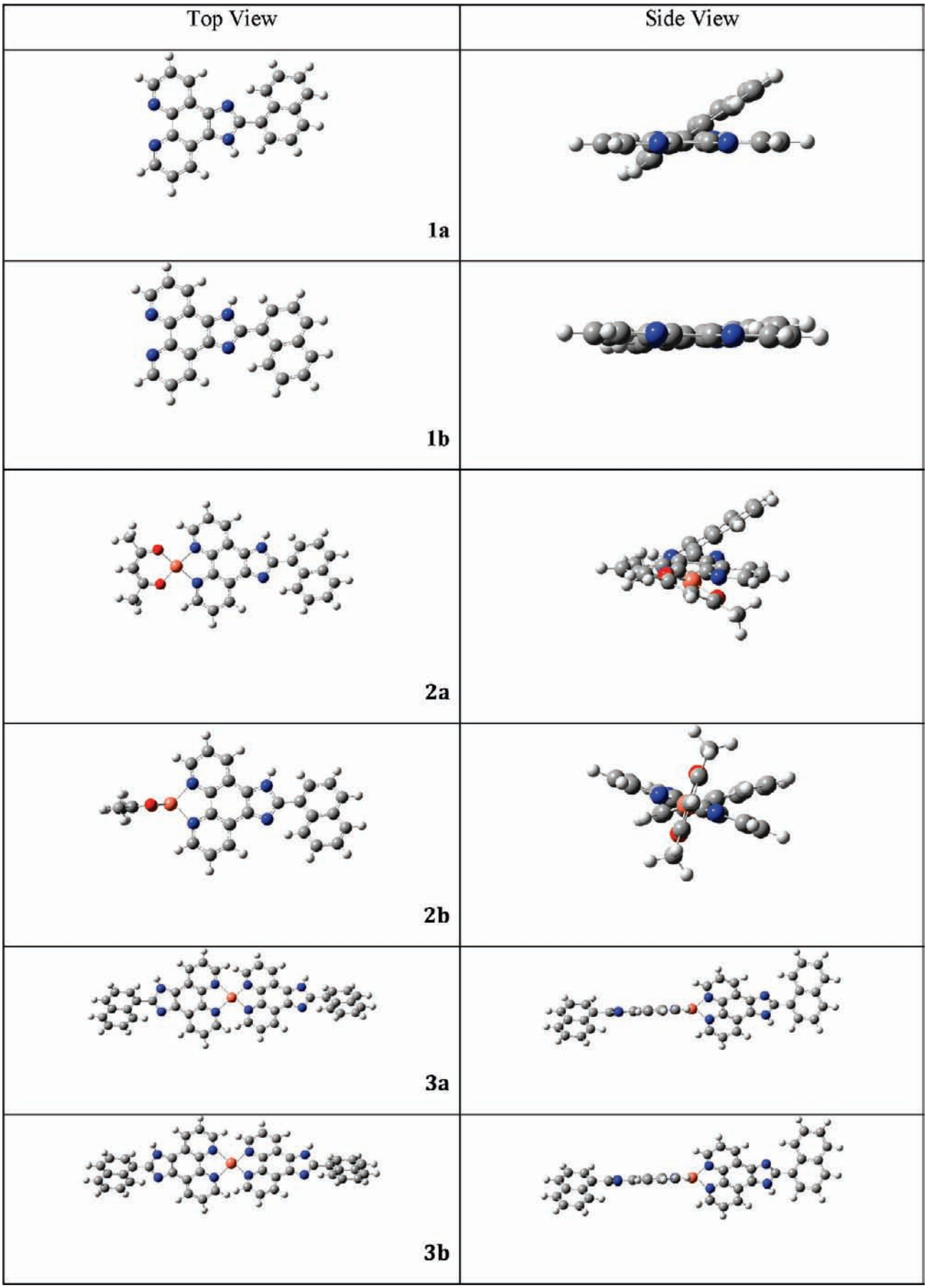

Figure 3. B3LYP/6-31G(d, p) optimized geometries: (a) ground state and (b) lowest exited states of **1**, **2**, and **3**.

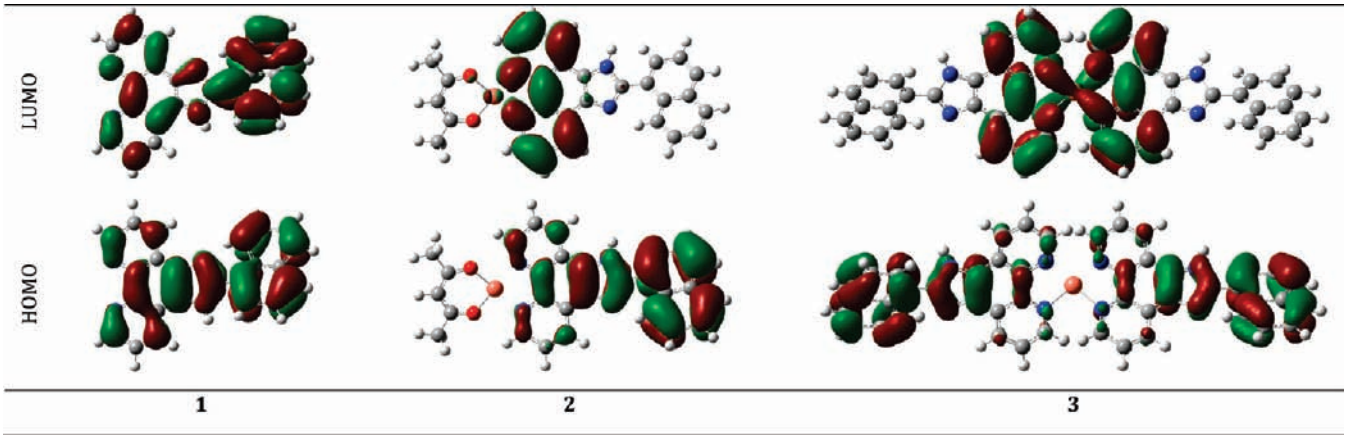

Figure 4. Frontier orbitals of **1**, **2**, and **3** with isovalued surface of 0.03 au.

Table 3. EPR Spectral Data of Copper(II) Complexes

complex	$g_{\parallel}$	$g_{\perp}$	$A_{\parallel}$G	$A_{\perp}$G
[Cu(acac)(nip)](NO_3) (**2**)	2.717	1.98	305	132
[Cu(nip)$_2$](NO_3)$_2$ (**3**)	2.589	2.00	300	220

is exactly reverse of that. On complexation with Cu(II), the naphthalene ring in the ligand rotates through 49.43° to form a completely planar molecule **2** (Figure 1), resulting in fluorescence quenching. Therefore, to find out the reason behind the fluorescence quenching upon complexation, we have carried out TDDFT calculations in gas phase, as well as in DMSO solvent.

Electronic Structure Calculations. B3LYP-optimized geometries of **1**−**3** in their ground state are shown in Supporting Information, Figure S11. The selected bond distances and angles are reported in Table S3 of the Supporting Information. As may be noticed, the naphthalene and the phenanthroline moieties in **1** orient mutually at an angle of 34°. On complexation with nip and acac, 1,10-phenanthroline ring is pushed below ~21° of "acac". The complexation in **3** facilitates two phenanthroline moieties to orient at an angle of ~44° in its ground state.

Optimized geometries in the lowest excited states derived from TD-DFT calculations are displayed in Figure 3. It may be remarked here that **2** attains near tetrahedral coordination for Cu^{2+} ion in its lowest excited state. In other words, transformation in the local coordination of Cu^{2+} in complex **2** from square planar in its ground state to tetrahedral geometry in the lowest excited state may be responsible for reduction in fluorescence intensity. Frontier orbital HOMO−LUMO energy difference in the ground states of **2** and **3** has been predicted to be 3.43 and 3.27 eV, respectively, and (cf. Table 4S of Supporting Information) are not influenced significantly on excitation.

Frontier orbitals HOMO and LUMO of **1**−**3** are displayed in Figure 4. Thus, it is apparent that the HOMO of **2** has largely been localized on naphthalene moiety and only partly on phenanthroline ring. Moreover, on excitation, charge transfer from naphthalene to phenanthroline can be noticed, and thus the LUMO exhibits electron-rich regions near phenanthroline. Similar inferences may be drawn in the case of **3**.

Electron Paramagnetic Resonance. EPR spectra for the polycrystalline complexes (**2** and **3**) are characterized by an axial g tensor at room temperature. Hyperfine features

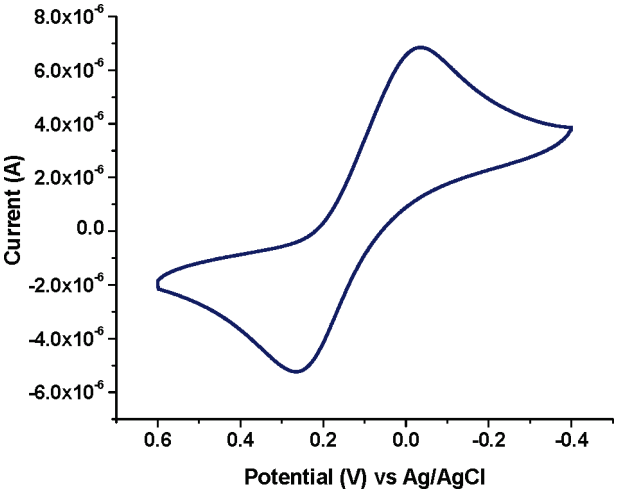

Figure 5. Cyclic voltammogram of **3** in DMSO (0.1 M $(Et_4N)ClO_4$) obtained at a glassy carbon electrode at scan rate of 100 mV s^{-1}.

due to copper ($S = {}^1/_2$ and $I = {}^3/_2$) could be resolved at 77 K in DMF glass in the parallel region for both the complexes. The molecular g values for the frozen solutions of metal complexes (Table 3) with $g_{\parallel} > g_{\perp}$ indicate that the unpaired electron occupies a formal $d_{x^2-y^2}$ orbital. The EPR spectrum of **2** in a DMF glass at 77 K (Supporting Information, Figure S5) shows distinct ligand hyperfine splittings, barely resolved for the $g_{\perp}$ lines but clearly so at $g_{\parallel}$ with two equivalent ^{14}N nuclei ($I = 1$ with $A_N = (22.8, 28.8, \text{and } 36.8) \times 10^{-4}$ cm^{-1}).

Electrochemistry. Cyclic voltammetry of complexes **2** and **3** was performed with a glassy carbon electrode at a scan rate of 100 mV s^{-1} in dimethyl sulfoxide containing tetraethyl ammonium perchlorate (0.1 M) as supporting electrolyte. The cyclic voltammogram of complex **3** is shown in Figure 5. The complexes are redox active and show quasi-reversible cyclic voltammetric response, which can be assigned to the Cu^{II}/Cu^{I} couple at 0.266 and 0.145 V vs Ag/AgCl for complexes **2** and **3**, respectively. The redox potential for complex **3** is relatively higher than that for **2**, which is attributed to the extension of the corresponding π framework around the metal center.[49]

(49) Gupta, T.; Dhar, S.; Nethaji, M.; Chakravarty, A. *Dalton Trans.* **2004**, 1896–1900.

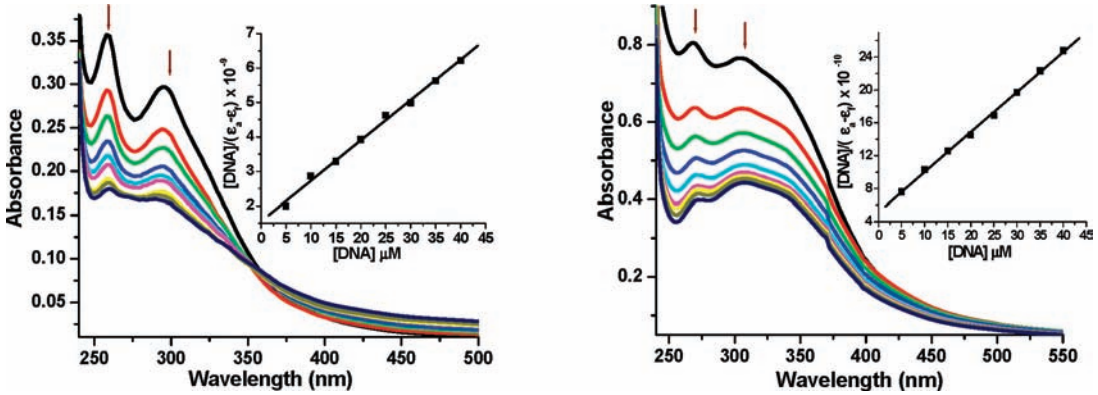

Figure 6. Changes in the electronic absorption spectra of **2** and **3** (20 μM) with increasing concentrations (0−40 μM) of CT-DNA (phosphate buffer, pH 7.2); the inset shows a fitting of the absorbance data at 296 nm for **2** and 306 nm for **3** used to obtain the binding constants.

Table 4. Electronic Absorption Data upon Addition of CT-DNA

complexes[a]	$\Delta\lambda_{max}$ (nm)	hypochromism,[b] H (%)	K_b[b] (M^{-1})
2	6 (296), 2 (258)	43.3 (296), 49.5 (258)	7.5×10^4
3	4 (304), 8 (268)	42.1 (304), 50.5 (268)	9.69×10^4
[Cu(imda)(dpq)][c]	1 (258)	63 (258)	1.7×10^4
[Cu(tdp)(dpq)][d]	1 (256)	54 (256)	9.1×10^5
$[Pt(en)(nip)]^{2+}$[e]	16 (302)	41.8 (302)	2.80×10^5
$[Ru(bpy)_2(BPIP)]^{2+}$[f]	7 (467)	39.4 (467)	1.7×10^5
$[Ru(phen)_2(BPIP)]^{2+}$[f]	6 (465)	30.6 (465)	7.03×10^4
$[Co(phen)_2(HPIP)]^{3+}$[g]	7 (274)	47.1 (274)	4.1×10^5
$[Co(phen)_2(HNAIP)]^{3+}$[g]	3 (273)	25.0 (273)	1.8×10^5

[a] [Cu] = 20 μM. [b] H % = 100($A_{free} - A_{bound}$)/A_{free} in phosphate buffer (pH = 7.2) where A = absorbance. Error limit: λ_{max} = ±2 nm, H (%) = ±5%; K_b (M^{-1}) = ±5%. [c] Reference 16. [d] Reference 22. [e] Reference 53. [f] Reference 26. [g] Reference 28.

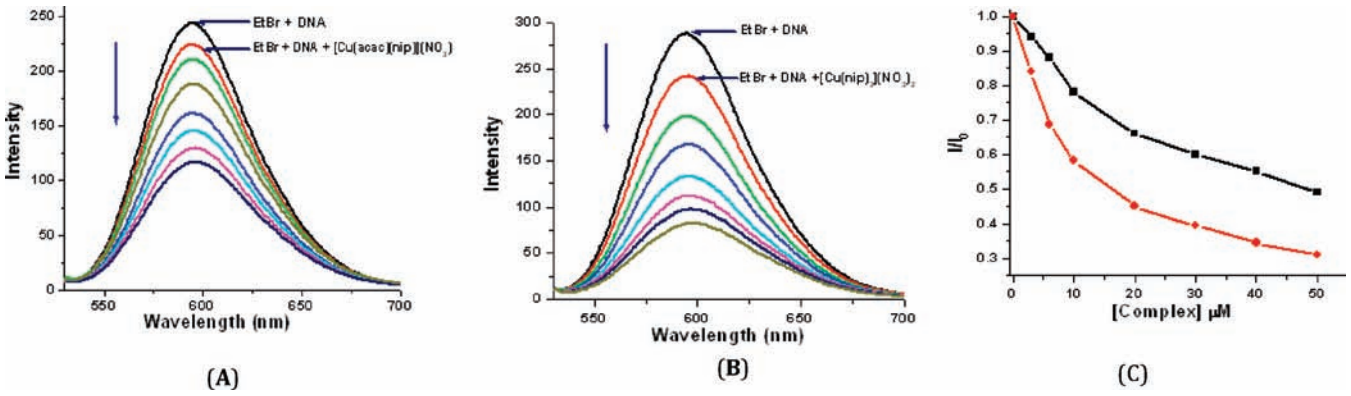

Figure 7. Effect of addition of (A) **2** and (B) **3** on the emission intensity of the CT DNA-bound ethidium bromide (20 μM) at different concentrations in a 20% DMF phosphate buffer (pH 7.2). (C) Plots of relative integrated emission intensity versus [DNA]/[Cu] for **2** (■) and **3** (●).

DNA Binding Studies. Absorption Spectral Studies. Monitoring the changes in absorption spectrum of the metal complexes upon addition of increasing amounts of DNA is one of the most widely used methods for determining overall binding constants. A complex binding to DNA through intercalation usually results in hypochromism and bathochromism involving strong stacking interaction between an aromatic chromophore and the base pairs of DNA. Upon addition of calf-thymus DNA to **2** and **3**, there is a decrease in molar absorptivity (hypochromism, 40−50%) of the intense intraligand (IL) absorption bands (240−400 nm) of complexes (Figure 6). For **3**, hypochromism is about 42.1% (304 nm) and 50.5% (268 nm), and for **2** it is 43.3% (296 nm) and 49.5% (258 nm) indicating strong binding of these complexes with DNA;[50−52] the percentage of hypochromism and red shifts are listed in Table 4.

In order to compare the DNA-binding affinities of these complexes quantitatively, their intrinsic binding constants with CT-DNA were obtained by monitoring the changes in absorption at intraligand band (Figure 6) with increasing concentrations of DNA using eq 2 and were found to be

(50) Tysoe, S. A.; Morgan, R. J.; Baker, A. D.; Strekas, T. C. *J. Phys. Chem.* **1993**, *97*, 1707–1711.
(51) Kelly, J. M.; Tossi, A. B.; McConnell, D. J.; OhUigin, C. *Nucleic Acids Res.* **1985**, *13*, 6017–6034.
(52) Haworth, I. S.; Elcock, A. H.; Freemann, J.; Rodger, A.; Richards, W. G. J. *J. Biomol. Struct. Dyn.* **1991**, *9*, 23–44.

7.5×10^4 and 9.69×10^4 for **2** and **3**, respectively, indicating their strong binding to DNA, which is consistent with other reported intercalating Cu(II),[22] Ru(II),[26] Co(III),[28] and Pt(II)[53] complexes.

Ethidium Bromide Displacement Assay. The competitive DNA binding of complexes has been studied by monitoring changes in emission intensity of ethidium bromide (EtBr) bound to CT-DNA as a function of added complex concentration. Though the emission intensity of EtBr in buffer medium is quenched by the solvent molecules,[54,55] it is enhanced by its stacking interaction between adjacent DNA base pairs. When complexes **2** and **3** were added to DNA pretreated with EtBr {[DNA]/[EtBr] = 1:1}, the DNA-induced emission intensity of EtBr was decreased (Figure 7). Addition of a second DNA binding molecule would quench the EtBr emission by either replacing the DNA-bound EtBr (if it binds to DNA more strongly than EtBr) or accepting an excited state electron from EtBr. Because the complexes **2** and **3** have planar ligands, they efficiently compete with strong intercalators like EtBr for intercalative binding sites on DNA by replacing EtBr, which is reflected in quenching of emission intensity of DNA-bound EtBr. The apparent binding constant (K_{app}) has been calculated from the eq 3.[56]

$$K_{EtBr}[EtBr] = K_{app}[complex] \quad (3)$$

where K_{EtBr} is $1 \times 10^7\ M^{-1}$ and the concentration of EtBr is 20 μM; [complex] is the concentration of the complex causing 50% reduction in the emission intensity of EtBr. The K_{app} values for **2** and **3** are $4.0 \times 10^6 \pm 0.2$ and $6.6 \times 10^6 \pm 0.6\ M^{-1}$, respectively. The higher values of K_{app} indicate that these complexes bind to DNA by intercalation.

DNA Thermal Denaturation. Further evidence for the intercalation of the complexes into the helix was obtained from the DNA melting studies. Interaction of the aromatic chromophore of the metal complex into the double helix is known to increase the helix melting temperature (T_m), the temperature at which the double helix denatures into single-stranded DNA.[57] The extinction coefficient of DNA bases at 260 nm in the double strand is much less than that in the single-stranded form. Hence, melting of the helix leads to an increase in the absorption at this wavelength. CT-DNA was seen to melt at 58 ± 1 °C (phosphate buffer) in the absence of complex. The melting temperature of DNA increased by 9 and 13 °C for **2** and **3**, respectively, which is typical of intercalating metal complexes (10−14 ± 1 °C),[58,59] which indicates that **3** binds strongly compared with **2**. This behavior is comparable to classical intercalators.

Viscosity Measurement. To further clarify the nature of the interaction between the complexes and DNA, viscosity measurements were carried out. Optical photophysical probes provide necessary but not sufficient, evidence to support the binding mode of the copper(II) complexes to DNA. Hydrodynamic measurements are sensitive to change in length of DNA and considered to be the most critical and least ambiguous tests in evaluating binding modes in solution in the absence of crystallographic structural data.[60,61] Lengthening of DNA helix occurs on intercalation as base pairs are separated to accommodate the binding ligand leading to increase in DNA viscosity. Partial or nonclassical intercalation of ligand may bend or kink the DNA helix, thereby decreasing its effective length and subsequently viscosity.

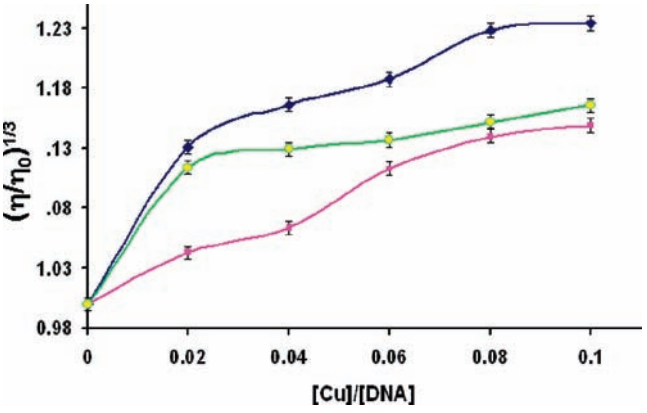

Figure 8. Effect of increasing amount of the (◆) EtBr, (●) **2**, and (■) **3** on the relative viscosities of calf thymus DNA at 28 °C, [DNA] = 200 μM. The results are the mean of three independent experiments carried out under identical conditions.

The values of relative specific viscosities of DNA in the absence and presence of complexes are plotted against [complex]/[DNA]. The relative viscosities of CT-DNA bound to **2** and **3** increased with increasing complex concentration (Figure 8) similar to some known intercalators,[62] indicative of a classical intercalation.

DNA Cleavage without Added Reagents. To assess the DNA cleavage ability of the complexes, supercoiled (SC) plasmid pBR322 DNA (100 ng/μL) was incubated with varying concentrations of complexes in 5% DMF in TBE buffer at pH 8.2 for 30 min in the concentration range of 10−100 μM. It was observed (Figure 9) that at higher concentrations, there is a change in the electophoretic mobility of the nc form eventually leading to condensation of DNA. The process of DNA condensation seems to start above 20 μM concentration in both complexes but the extent of condensation was more prominent in **3** due to presence of two nip ligands with high $\pi-\pi$-stacking interactions and greater positive charge (+2) compared with **2** with one positive charge and one nip ligand.

When inhibitors of oxygen-based radicals were added to the reaction mixture to establish the reactive species responsible for DNA cleavage (Figure 10, Table S5, Supporting Information), it was observed that DNA cleavage by **2** was not affected in the presence of DMSO and mannitol suggesting that hydroxyl radicals are not involved

(53) Kieltyka, R.; Fakhoury, J.; Moitessier, N.; Sleiman, H. F. *Chem.—Eur. J.* **2008**, *14*, 1145–1154.
(54) Waring, M. J. *J. Mol. Biol.* **1965**, *13*, 269–282.
(55) Changzheng, I.; Jigui, W.; Liufang, W.; Min, R.; Naiyang, J.; Jie, G. *J. Inorg. Biochem.* **1999**, *73*, 195–202.
(56) Lee, M.; Rhodes, A. L.; Wyatt, M. D.; Forrow, S.; Hartley, J. A. *Biochemistry* **1993**, *32*, 4237–4245.
(57) Cusumano, M.; Giannetto, A. *J. Inorg. Biochem.* **1997**, *65*, 137–144.
(58) Neyhart, G. A.; Grover, N.; Smith, S. R.; Kalsbeck, W.; Fairley, T. A.; Cory, M.; Thorp, H. H. *J. Am. Chem. Soc.* **1993**, *115*, 4423–4428.
(59) Selvakumar, B.; Rajendiran, V.; Maheswari, P. U.; Stoeckli- Evans, H.; Palaniandavar, M. *J. Inorg. Biochem.* **2006**, *100*, 316–330.
(60) Satyanarayana, S.; Dabrowiak, J. C.; Chaires, J. B. *Biochemistry* **1993**, *32*, 2573–2584.
(61) Satyanarayana, S.; Dabrowiak, J. C.; Chaires, J. B. *Biochemistry* **1992**, *31*, 9319–9324.
(62) Kumar, C. V.; Asuncion, E. H. *J. Am. Chem. Soc.* **1993**, *115*, 8547–8553.

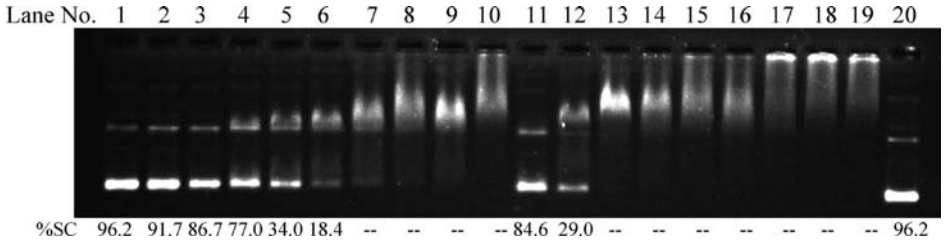

Figure 9. Agarose (1%) gel electrophoresis showing concentration-dependent cleavage of pBR322 DNA by **2** and **3** at 10−100 μM, [DNA] = 300 ng, incubation time = 30 min at 37 °C in TBE buffer, pH 8.2. Lanes 1 and 20, DNA control; lane 2, DNA + **2** (10 μM); lane 3, DNA + **2** (20 μM); lane 4, DNA + **2** (30 μM); lane 5, DNA + **2** (40 μM); lane 6, DNA + **2** (50 μM); lane 7, DNA + **2** (60 μM); lane 8, DNA + **2** (70 μM); lane 9, DNA + **2** (80 μM); lane 10, DNA + **2** (100 μM); lane 11, DNA + **3** (10 μM); lane 12, DNA + **3** (20 μM); lane 13, DNA + **3** (30 μM); lane 14, DNA + **3** (40 μM); lane 15, DNA + **3** (50 μM); lane 16, DNA + **3** (60 μM); lane 17, DNA + **3** (70 μM); lane 18, DNA + **3** (80 μM); lane 19, DNA + **3** (100 μM).

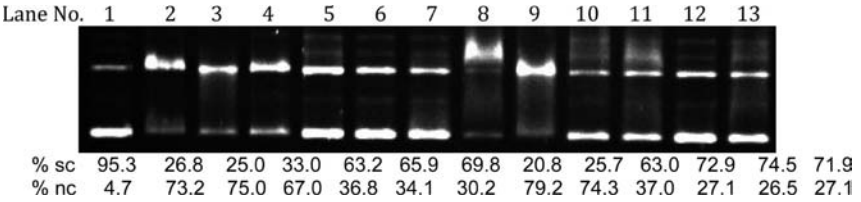

Figure 10. Agarose (1%) gel showing the effect of inhibitors on cleavage of pBR322 plasmid DNA by **2** and **3**. [DNA] = 300 ng, [**2**] = 40 μM, and [**3**] = 20 μM. Lane 1, DNA control; lane 2, DNA + **2**; lane 3, DNA + **2** + DMSO (1 mM); lane 4, DNA + **2** + mannitol (50 mM); lane 5, DNA + **2** + DABCO (10 mM); lane 6, DNA + **2** + L-histidine (20 mM); lane 7, DNA+ **2** + SOD (15 units); lane 8, DNA + **3**; lane 9, DNA + **3** + DMSO (1 mM); lane 10, DNA + **3** + mannitol (50 mM); lane 11, DNA + **3** + DABCO (10 mM); lane 12, DNA + **3** + L-histidine (20 mM); lane 13, DNA + **3** + SOD (15 units).

Table 5. Stern−Volmer Quenching Constants for the Interaction of **2** and **3** with BSA at Different Temperatures

temp (K)	**2** (mol^{-1})	**3** (mol^{-1})
298	6.9×10^4	1.38×10^5
305	7.7×10^4	1.48×10^5
313	8.7×10^4	1.53×10^5

in DNA cleavage. Further, the cleavage reactions were found to be inhibited by singlet oxygen scavengers DABCO and L-histidine (Figure 10, lane 6, 38.2% ± 1.9% and lane 7, 41.0% ± 3%, respectively) and superoxide radical scavenger, SOD (lane 8, 45.12% ± 2.5%), revealing that singlet oxygen and superoxide radicals are the major species responsible for DNA cleavage by **2**. Similarly, DABCO, L-histidine, and SOD (lanes 11−13; 54.73% ± 1.6%, 56.35% ± 0.6% and 53.62% ± 1.0%, respectively) were found to inhibit DNA cleavage by **3**, suggesting the involvement of singlet oxygen and superoxide radicals. Some inhibition was also observed by mannitol (lane 10, 44.28% ± 4.2%), a hydroxyl radical scavenger, in case of **3**.

BSA Interaction Studies. The tryptophan emission-quenching experiments were carried out using bovine serum albumin (BSA) in the presence of **2** and **3** to investigate their interaction with proteins. The emission intensity depends on the degree of exposure of the two tryptophan side chains, 134 and 212, to polar solvent and also on its proximity to specific quenching groups, such as protonated carbonyl, protonated imidazole, deprotonated ε-amino groups, and tyrosinate anions. The quenching of emission intensity of BSA was observed in presence of **2** and **3** because of possible changes in protein secondary structure leading to changes in tryptophan environment of BSA.[63] Quenching of fluorescence of BSA by complexes is either by a dynamic or by a static mechanism. Dynamic quenching refers to a process in which fluorophore and the quencher come in contact during the transient existence of the excited state while, static quenching refers to fluorophore−quencher complex formation. The dynamic and static quenching can be differentiated by their temperature dependence. Dynamic quenching depends on the diffusion coefficient. Hence, increase in temperature results in higher diffusion coefficient and the bimolecular quenching constant is expected to be increased with increase in temperature. In contrast, in static quenching, increased temperature is likely to decrease the fluorophore−quencher stability constant resulting in lower values of quenching constants.[64] We have measured the Stern−Volmer quenching constants at various temperatures. These results show that the quenching constant increases with increase in temperature indicating the dynamic quenching mechanism (Table 5). Further, the higher slope for **3** in the plot of I/I_0 versus [complex] (Figure 11) reveals the stronger protein-binding ability of the complex **3** with enhanced hydrophobicity.

Anticancer Activity Studies. The anticancer activities of compounds **1**−**3** toward human MCF-7, HeLa, and HL-60 cancer cell lines and MCF-12A (normal cell line) have been examined in comparison with the currently used drug paclitaxel under identical conditions by using MTT assay. It is found that the compounds exhibit significant cytotoxic activities in a time-dependent manner. The ability of the drugs to induce either apoptosis or necrosis seems to be a primary factor in determining their efficacy. However, the major challenging aspect of synthesizing new chemotherapeutic agents is selectivity toward cancerous cells compared with the normal cells. Therefore, we have studied the cytotoxic efficacy induced by **1**−**3** on MCF-12A normal epithelial cell line. Gel electrophoresis was carried out for detecting DNA fragmentation,

(63) Zhang, Ye-Z.; Zhang, X-P; Hou, H.-N.; Dai, J.; Liu, Y. *Biol. Trace Elem. Res.* **2008**, *121*, 276–287.

(64) Hu, Y. J.; Liu, Y.; Pi, Z. B.; Qu, S. S. *Bioorg. Med. Chem.* **2005**, *13*, 6609–6614.

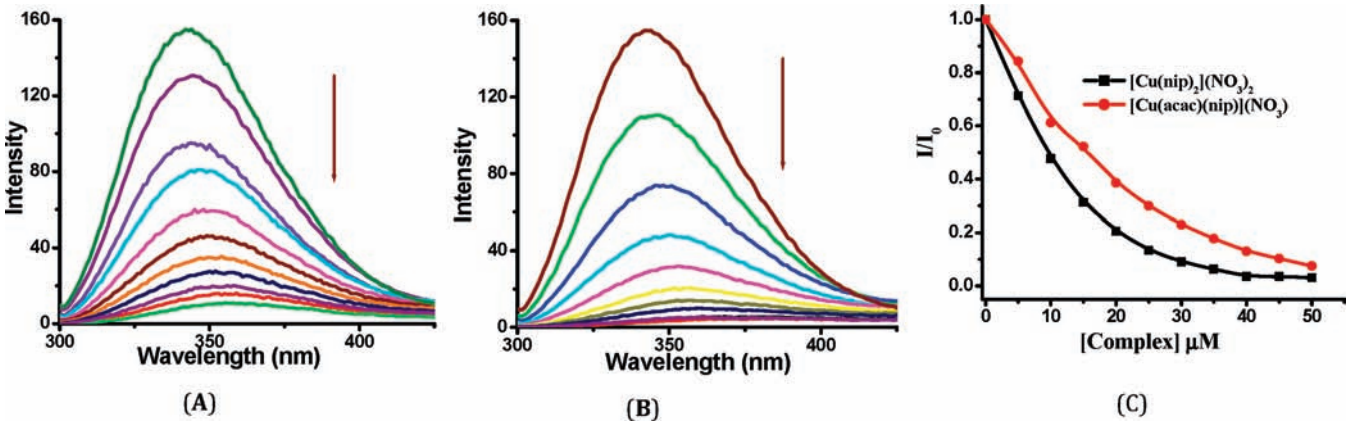

Figure 11. Effect of addition of (A) **2** and (B) **3** on the emission intensity of the BSA (50 μM) at different concentrations in a 20% DMF phosphate buffer (pH 7.2). (C) Plots of relative integrated emission intensity versus [DNA]/[Cu] for (■) **2** and (●) **3**.

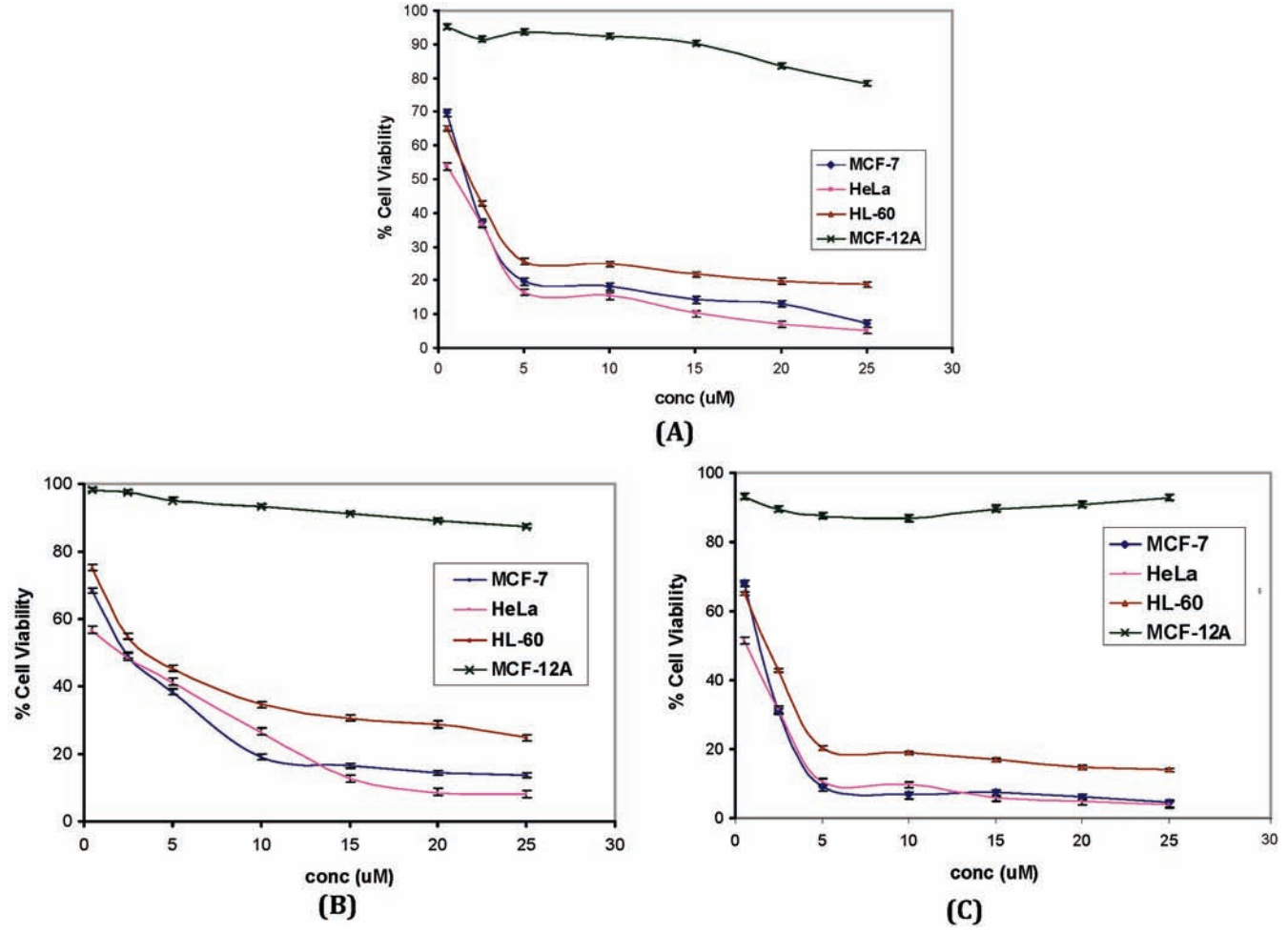

Figure 12. Effect of concentration (100 nM to 25 μM) on viability of cancer cells by (A) **1**, (B) **2**, and (C) **3** on 24 h incubation as determined by MTT assay. Results are mean of three independent experiments carried out under identical conditions.

and cellular uptake was monitored using fluorescence microscopy because the compounds have intrinsic fluorescence. The cellular uptake could be most likely due to the adherence of the positively charged metal complexes to the plasma membrane by electrostatic attraction before its transport across the membrane facilitated by difference in concentration gradient. The emission spectra of complexes show that there is greater excitation

Table 6. Comparative IC_{50} Values of **1**−**3** When Tested on MCF-7, HeLa, and HL-60 Cell Lines after 24 h

	IC_{50} (nM, 24 h)		
Compound	MCF-7	HeLa	HL-60
1	1640 ± 0.134	960 ± 0.375	2330 ± 0.087
2	3200 ± 0.032	1860 ± 0.076	3540 ± 0.365
3	1250 ± 0.253	800 ± 0.466	1522 ± 0.469
paclitaxel	135 ± 0.064	899 ± 0.357	1635 ± 0.385

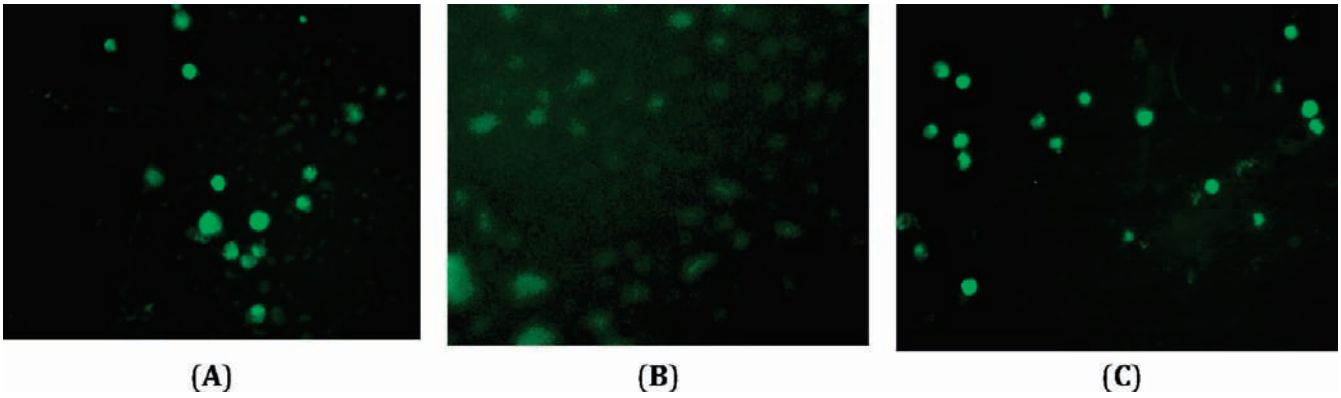

Figure 13. The cellular uptake studies to monitor the influx of (A) **1**, (B) **2**, and (C) **3** within MCF-7 cells after 24 h incubation in the dark. Images were taken in a Carl Zeiss Axio Scope, A1 fluorescence microscope with filter set no. 9, excitation at 450−490 nm.

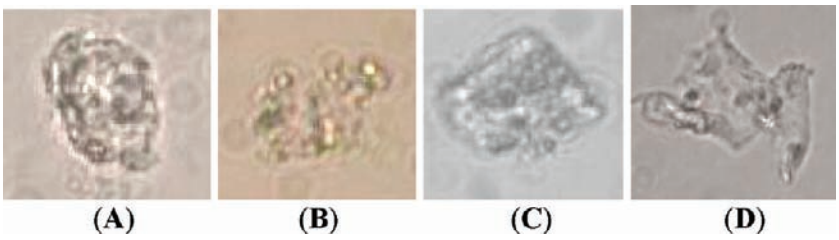

Figure 14. Ultrastructural analysis of isolated mitochondria. Micrographs were obtained after incubation of mitochondria isolated from HeLa cell lines: (A) untreated (control), (B) treated with **1**, (C) treated with **2**, (D) treated with **3**. Images were taken in a Carl Zeiss Axio Scope, A1 fluorescence microscope under normal mode.

at ~430 nm, which is a typical minimum excitation wavelength for single-photon confocal microscopy experiments.[65] Further, there is no overlap between the absorption and emission spectra of **1**−**3** which is an advantage for fluorescence microscopy, since the overlap of spectra results in interference of excitation light in collection of emission image, which decreases the image contrast.[65]

The compounds exhibited the apoptotic mode of cell death in the region 0−50 μM. When higher concentrations of these compounds (greater than 100 μM) were used, necrosis was observed within 24 h. Thus, a narrow concentration range (100 nM to 25 μM) was selected for testing cell viability. Figure 12a−c depicts the cytotoxicities of compounds **1**−**3** after 24 h incubation. The IC_{50} values against three cell lines, MCF-7, HeLa, and HL-60, is shown in Table 6. Compound **3** is remarkable in displaying the most prominent cytotoxicity against the HeLa cell line (IC_{50} = 800 nM after 24 h, Table 6) with its activity equal to cisplatin.[66] Compounds **1**−**3** show ~85−95% cell viability in the MCF-12A cell line (Supporting Information, Figure S9); thus the compounds are selective toward cancerous cells.

The results of gel electrophoresis assay show the absence of DNA ladder formation (Supporting Information, Figure S10); instead a smear is observed for all three compounds. Cells that undergo mitotic catastrophe usually fail to show DNA ladder formation.[21] Complex **3** possesses a very prominent cytotoxicity, which is consistent with its strong DNA binding involving hydrophobic forces of interaction and efficient DNA cleavage.

In cells incubated with **1** and **3**, high levels of fluorescence were observed within the cells, while this is not the case in cells incubated with **2** (Figure 13). The cytotoxicity data shows the role of this compound in induction of cell death. This means that **2** is causing cell death by an alternative mechanism, which could be disruption of lysosomes, which has long been identified as trigger for cell death.[34] Such lysosomally-induced apoptosis could be an explanation for the cytotoxicity and more diffused distribution of fluorescence in the cells. Recently it has been reported that disruption of lysosomes results in the release of its acidic content into cytoplasm which in turn causes disruption of plasma membrane leading to cell death.[67] After 48 h, **2** shows cell death similar to that from **1**. To ascertain the apoptotic mode of cell death, mitochondrial membrane permeability was studied.

Mitochondrial Membrane Permeability. Mitochondria from HeLa cell lines were purified as described by Buron et al.[68] Ultrastructural comparative studies of isolated mitochondria from the HeLa cell line (untreated) reveal a matrix/cristae organization. On treatment with compounds **1**−**3**, the outer wall is disrupted relatively more in the case of **1** and **3** compared with **2** (Figure 14). This observation is indicative of the apoptotic mode of cell death via the mitochrondrial pathway.[69] Further investigations

(65) Hibbs, A. R. *Confocal Microscopy for Biologists*; Plenum Publishers, New York, 2004.
(66) Kalinowska-Lis, U.; Ochocki, J.; Matlawska-Wasowska, K. *Coord. Chem. Rev.* **2008**, *252*, 1328–1345.
(67) Hall, M. D.; Foran, G. J.; Zhang, M.; Beale, P. J.; Hambley, T. W. *J. Am. Chem. Soc.* **2003**, *125*, 7524–7525.
(68) Buron, N.; Porceddu, M.; Brabant, M.; Desgue, D.; Racoeur, C.; Lassalle, M.; Péchoux, C.; Rustin, P.; Jacotot, E.; Borgne-Sanchez, A. *PLoS One* **2010**, *5*, 1–13.
(69) Marchetti, P.; Castedo, M.; Susin, S. A.; Zamzami, N.; Hirsch, T.; Macho, A.; Haeffner, A.; Hirsch, F; Geuskens, M.; Kroemer, G *J. Exp. Med.* **1996**, *184*, 1155–1160.

detailing the underlying mechanism are currently underway in our laboratory.

Conclusions

In conclusion, we have synthesized fluorophore-labeled copper(II) complexes and characterized them by usual spectroscopic techniques. Density functional calculations reveal near square planar geometry for $[Cu(nip)(acac)]^+$ in consonant with that observed from the X-ray crystal structure. Unlike for $[Cu(nip)_2]^{2+}$ complex, the change of square planar geometry to tetrahedral was noticed in $[Cu(nip)(acac)]^+$ complex in lowest excited state. Complexes **2** and **3** bind to DNA through intercalation with binding constants of the order of 10^4. They cleave plasmid pBR322 DNA without addition of any external additives by an oxidative mechanism. They bind to bovine serum albumin and are responsible for quenching of BSA fluorescence by dynamic quenching mechanism. All compounds are highly active and selective toward cancer cells, and their cellular uptake could be monitored by fluorescence microscopy due to their inherent fluorescence, which is ligand-based.

Acknowledgment. S.S.B. acknowledges Department of Science and Technology (DST), New Delhi, India, for providing a fellowship under the scheme SR/S5/BC-25/2006. Anupa Kumbhar acknowledges the financial assistance by BCUD Seed Money, University of Pune (Univ. Ref. No. BCUD/92). The financial support in the form of Fast Track Project for Young Scientists by Department of Science and Technology (SR/FTP/CS-96/2007) to Aayesha Khan is gratefully acknowledged. Thanks are also due to RSIC IIT, Bombay, for recording EPR spectra and SAIF, Central Drug and Research Institute (CDRI), Lucknow, for CHN and ESI-MS analyses. Authors thank Dr. A. S. Kumbhar for cyclic voltammetric and DNA melting measurements.

Supporting Information Available: Selected bond lengths [Å] and angles [deg] for **1** and **2**, selected geometrical parameters for **1**−**3**, HOMO−LUMO energy gaps in ground and first excited state of **1**−**3** (in eV), percentage cleavage data of pBR322 DNA by complexes **2** and **3** on treatment with ROS inhibitors, figure showing $\pi-\pi$ interactions between the two molecules of **1**, the H-bonding of lattice nitrates and $\pi-\pi$ interactions in **2**, overlap of **1** and **2** showing the change in orientation of naphthalene ring in **1** on binding to Cu(II) making it almost planar, cyclic voltammogram of **2**, EPR spectra of **2** and **3**, plots of concentration-dependent DNA cleavage by **2**, effect of temperature on Stern−Volmer quenching constant of **2** and **3**, MCF-7 cells (a) control cells and (b) cells treated with DMSO vehicle control, effect of **3** on normal epithelial cell line MCF-12A, agarose gel showing smearing of DNA extracted from the cells incubated with **1**, **2**, and **3**, optimized structures of **1**, **2**, and **3**. This material is available free of charge via the Internet at http://pubs.acs.org. CCDC 782183 and CCDC 782182 contain the supplementary crystallographic data for **1** and **2**, respectively. The data can be obtained free of charge via www.ccdc.cam.ac.uk/conts/retrieving.html (or from the Cambridge Crystallographic Data Centre, 12 Union Road, Cambridge CB2 1EZ, UK; fax (+44)1223-336-033 or e-mail deposit@ccdc.cam.uk).